Modelling and Simulation of Mechanical Behaviour of an Ultra-Long Porous Silicon Neural Microelectrode

Rayan Fayad, Soumaya Berro, Bakri AbdulHay, Houssein Hajj-Hassan, Hassan M. Khachfe, Mohamad Hajj-Hassan
Dept. of Biomedical Engineering
Lebanese International University
Beirut, Lebanon
{bakri.abdulhay, houssein.hajjhassan, hassan.khachfe, mohamad.hajjhassan}@liu.edu.lb

***Abstract*—Porous silicon has become the gold standard when it comes to improving biocompatibility and bioactivity. For this reason, it has become a primary candidate in neural electrodes research and development. Consequently, the purpose of this work was to investigate the mechanical strength of porous silicon neural electrodes. Thus, a finite element model representing the proposed electrode was generated. Mechanical simulation was done on porous and non-porous electrodes using COMSOL® Multiphysics. Results showed that porosity decreased the mechanical strength of the neural electrode without risking the mechanical requirements for neural applications.**

Keywords-biocompatiblity; finite element model; failure analysis; neural microelectrodes; porous silicon

I. INTRODUCTION

For centuries, people have fantasized about the possibility to communicate with the human brain to understand its structure and how it functions. In the recent decades, due to progresses in neuroscience and microtechnology, this fantasy became a reality with the introduction of neural electrodes. Neural electrodes are implantable micro-dimensional structures that enables a bidirectional communication between the brain and an outer electronic circuitry [1]. These electrodes are used in both recording action potentials from neurons and stimulating specific brain regions, which aid in the diagnosis and treatment of several brain diseases such as seizures, epilepsy, and migraine [2]. Such interfaces have applications in neuroscience research and brain-machine interfaces [3][4].

Several types of neural electrodes have been designed and developed to date. These electrodes can be classified under three main categories: metal wire based, silicon based, and polymer based neural electrodes. A metal-based electrode is composed of a metal wire entirely insulated except for its tip; it is left exposed acting as a recording site [5]. The drawback of this type is that only one recording site was available and any attempt to increase the number of recording sites would increase the overall size of the electrode which is not generally desired. This drawback was solved with the introduction of silicon based neural electrodes that emerged with the advances of microfabrication techniques. Silicon offers suitable biocompatibility and mechanical strength and allows the incorporation of multiple recording sites without increasing the overall size of the electrode. Another type is the polymer-based neural electrode characterized by improved flexibility and biocompatibility. However, it suffers from lack of rigidity which leads to less accurate neural targeting [6].

This article covers the simulation of the mechanical behavior of porous silicon neural electrode. The next section presents the major limitation of neural electrodes and the advantages of using porous silicon. Section III introduces the design of the proposed electrode. Section IV discusses the simulation strategy followed. Section V details the results yielded.

II. ADVANTAGES OF POROUS SILICON FOR NEURAL ELECTRODES

The major limitation facing the previously mentioned types is the resultant tissue response, which is provoked by the neural injury upon the implantation of the electrode. This tissue response threatens the long-term functioning of the neural electrode. The implantation of any neural electrode is always a traumatic procedure. When a neural electrode is inserted into the brain, it breaches the vasculature and kills the neurons in its path. This provokes the activation of an acute immune response, which is characterized by the recruitment and activation of glial cells whose role is to digest the cellular debris with enzymes. This gives rise to a chronic response. This response results in the formation of an encapsulation layer termed the “glial scar” around the electrode. This scar isolates the electrode from nearby neurons and these neurons are in turn pushed away from the recording sites the thing that leads to signal deterioration [5].

It has been proven that tissue response is highly dependent on the surface topography. That is to say that rough surfaces such as porous ones are more biocompatible than smooth surfaces [7]. Particularly, porous silicon has shown enhanced biocompatibility and bioactivity [8]-[10]. For instance, in a study performed by Hajj-Hassan et al. [10], the biocompatibility and bioactivity of porous silicon wafers (Si) was assessed by examining the survival and replication of mesenchymal stromal cells (MSC) isolated from the bone marrow of

Copyright (c) IARIA, 2014. ISBN: 978-1-61208-359-9

wild type mice. These results were compared with that of cells growing in 2D culture on tissue culture plastic (TCP) and on smooth titanium (SmTi), which is well known for its superiority (gold standard) for the manufacture of implants. In the first experiment performed, bone marrow derived MSC were seeded in porous silicon wafers etched to a depth of 20 µm (Si20) in 12 well plates and harvested after 3, 6 ,and 9 days of culture. Control cells plated at the same density on tissue culture plastic were harvested at 6 days and stained with toluidine blue to visualize the cells. Results showed that the Si20 substrate supported the MSC growth. Additionally, an Alamar Blue metabolic assay was used to analyze the metabolic activity of cells grown porous silicon substrates etched to a depth of 20 µm (Si20) or 30 µm (Si30) and compared with TCP or smooth titanium, which is a common implant material. Representative results of the Alamar Blue assay, shown in Figure 1(A), indicate a small increase in metabolic activity of the cells grown on Si20 and Si30 samples compared to smooth titanium and tissue culture plastic controls. The cell counts indicated a steady increase in numbers that appeared to be dependent on the substrate on which they were grown.

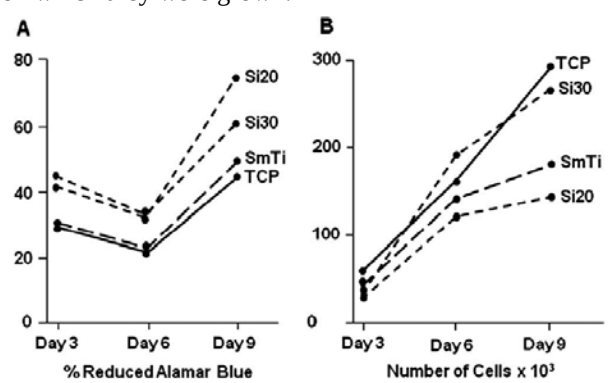

Figure 1. Quantitative analysis of MSC grown on porous silicon etched to a depth of 20 µm (Si20), 30 µm (Si30), commercial grade smooth titanium (SmTi) and tissue culture plastic (TCP) using the Alamar Blue assay to assess the metabolic activity [10].

So, it has been shown that the introduction of the pores improves the biocompatibility and bioactivity. However, a fundamental question imposes itself regarding whether their introduction influences the mechanical strength of the electrode. In other words, we are interested in knowing if the implanted porous electrode will still survive the forces exerted by the brain environment during and after implantation. The solution to this question is demonstrated in the sections that follow.

III. DESIGN

The following section covers the design of the proposed neural electrode. The developed neural electrode is constructed using a silicon substrate and is considered to be ultra-long with a length of 10.5 mm. Its overall structure is tapered, which facilitates the penetration. The geometry of the electrode is sectioned into three main regions; a base region, a measuring region incorporating the metal recording sites, and a piercing region. The relative dimensions of these regions are indicated in Figure 2. The electrode was implemented using COMSOL© Multiphysics 4.3 as depicted in Figure 3.

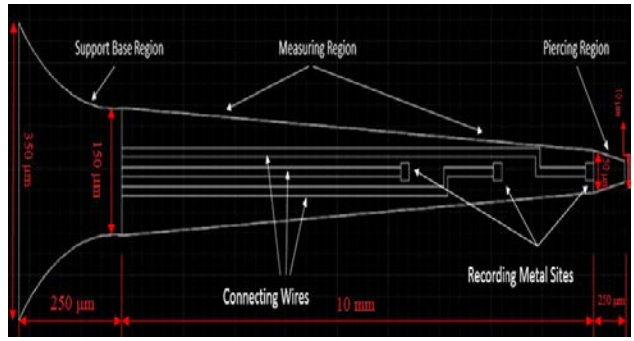

Figure 2. 2D drawing of the designed electrode with annotations.

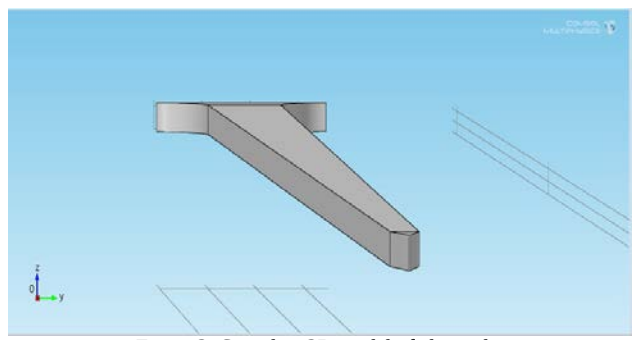

Figure 3. Complete 3D model of electrode.

As for the pores, they were characterized by a cylindrical geometry with a radius of 1.5 µm and a depth of 0.6 µm. This is illustrated in Figure 4.

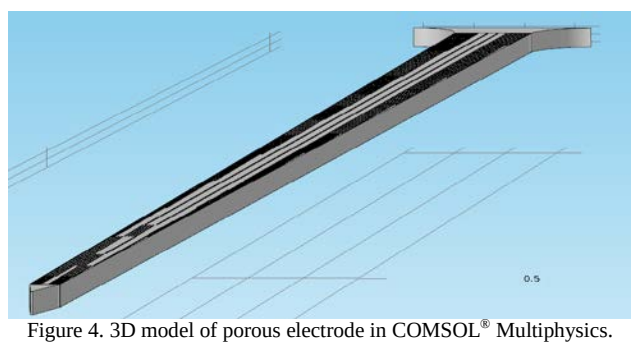

Figure 4. 3D model of porous electrode in COMSOL® Multiphysics.

Arrays of pores were distributed along the top surface of the electrode with a distance of 3 µm separating one pore and the other.

IV. SIMULATION STRATEGY

Regarding the adopted simulation strategy, increasing forces were gradually applied on both a porous and a non-porous electrodes until the failure stress of silicon, which is equivalent to 1GPa [11], is reached. During simulation,

two types of forces, which are naturally exerted by the brain environment, are applied on the electrodes [12]. The first force is vertical force that occurs as a result of the movement of the brain relative to the skull. This vertical force causes the bending of the electrode and is applied along the negative z-axis. The second force is an axial force that occurs during penetration and results in the buckling of the electrode. This force is applied along both the negative *x* and *y* axes. These forces were applied on the front face of the piercing tip while fixing the back face of the support base region as illustrated in Figure 5.

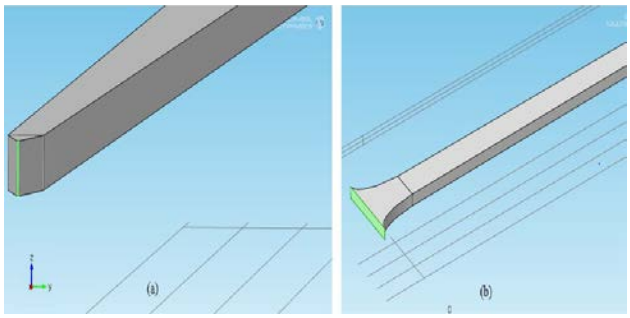

Figure 5. Marked in green is (a) Area on which the stress is applied, (b) area, which is a fixed constraint.

It is notable to mention that during the simulation of the porous electrode, pores were restricted to the weakest regions of the electrode as seen in Figure 6.

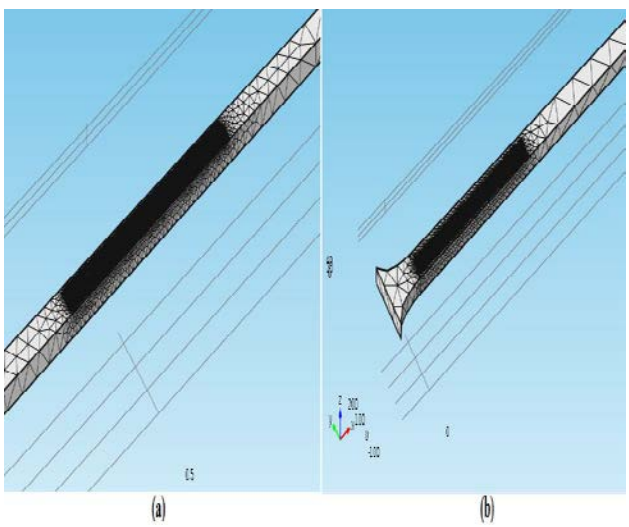

Figure 6. (a) Porous region on the middle of the probe, (b) porous region on the base.

This was done to reduce the computational complexity. These regions are the middle of the electrode (during axial loads), and the base region of the electrode (during vertical loads) [12].

V. Results and Discussion

The following section elaborates on the results obtained from the simulation of both the porous and non-porous electrodes. For each simulation, a plot of the induced principal stress in MPa versus the length of the electrode in µm as a result of applying axial and vertical loads.

Regarding the application of an axial force along the negative *x*-axis on the non-porous electrode, a force of 527.5 mN induced a maximum critical stress of 1GPa at a length of around 10.5 mm as indicated in the graph in Figure 7. This location corresponds to the tip region of the electrode. As for the porous electrode, a force of 522.5 mN induced a similar response at a similar location as shown in Figure 8.

Most importantly, it is essential to mention that the maximum critical stress is determined using the "Maximum Distortion Energy Theory" also known as the "*R. von Mises* Theory", which is demonstrated in equation 1 [13].

$$\sigma_e=(\sigma_1^2+\sigma_1\sigma_2+\sigma_2^2)^{1/2} \quad (1)$$

where σ_e is the effective stress or *von Mises* stress and $\sigma_{1,2}$ are the principal stresses. The maximum distortion energy theory is one of the famous failure theories for ductile material. This theory states that failure is predicted to occur in the multiaxial state of stress when the distortion energy per unit volume becomes equal to or exceeds the distortion energy per unit volume at the time of failure in a simple uniaxial stress test using a specimen of the same material [14]. In other words, a given structural material is safe as long as the maximum value of the distortion energy per unit volume in that material remains smaller than the maximum distortion energy per unit volume required to cause yield in a tensile test specified of the same material. The simulated effective stress is then compared to the yielding stress of the material.

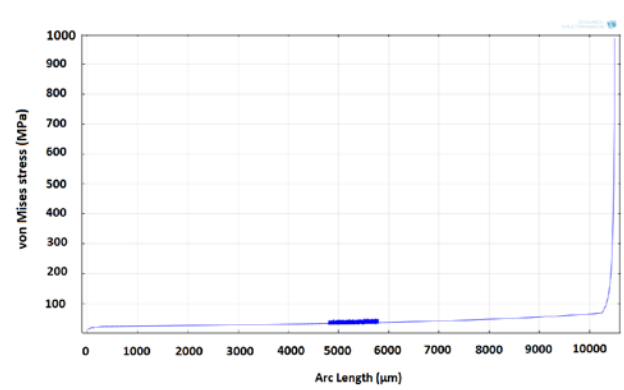

Figure 7. *Von Mises* stress induced upon applying an axial force along the negative *x*-axis versus the electrode length (non-porous).

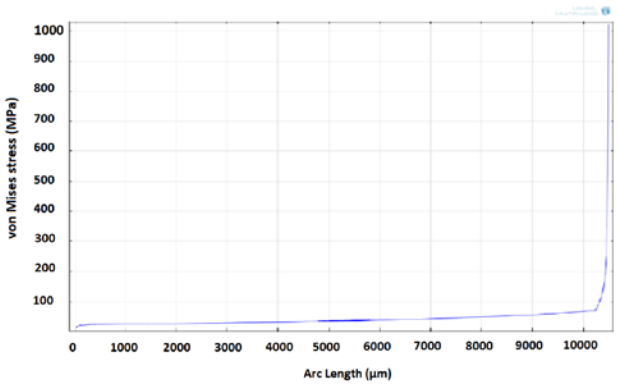

Figure 8. *Von Mises* stress induced upon applying an axial force along the negative *x*-axis versus the electrode length (porous).

As for the application of an axial force along the negative y-axis, for the non-porous electrode, a force of 47.5 mN, induced a maximum stress of 1GPa at a length of the electrode approximately equal to 5750 µm, which corresponds to the middle region of the electrode. Meanwhile, in the porous electrode, a force of 37.5 mN caused a fluctuation in the induced stress in the porous middle region. This region also incorporated the maximum stress of 1GPa. These results are indicated in the plots depicted in Figures 9 and 10, respectively.

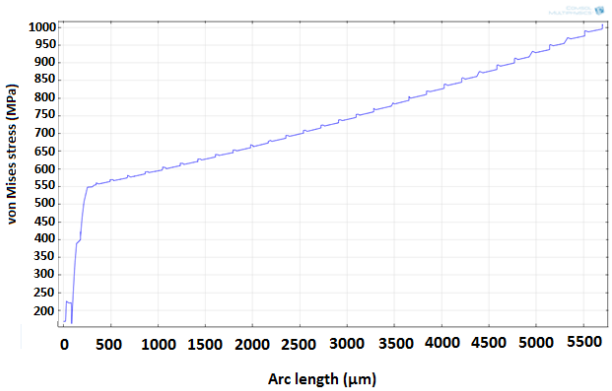

Figure 9: *Von Mises* stress induced upon applying an axial force along the negative y-axis versus the electrode length (non-porous).

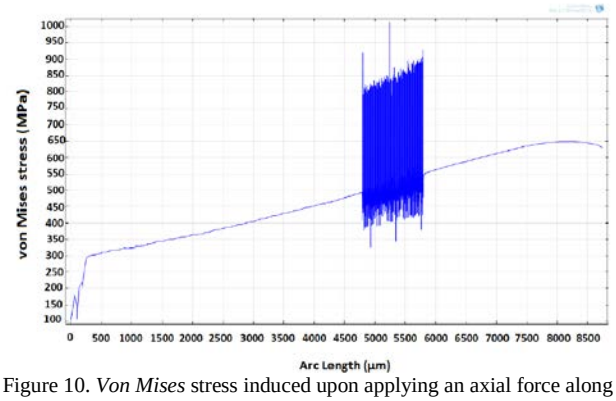

Figure 10. *Von Mises* stress induced upon applying an axial force along the negative y-axis versus the electrode length (porous).

Finally, regarding the application of a vertical force along the negative z-axis, for the non-porous electrode, a force of 18.25 mN, induced a maximum stress of 1GPa at a length of the electrode approximately equal to 400 µm which corresponds to the fixed base region of the electrode (Figure 11). On the other hand, in the porous electrode, a force of 11.5 mN caused a fluctuation in the induced stress in the porous base region. This region also contained the maximum stress of 1GPa (Figure 12). A summary of the results yielded is presented in Table 1.

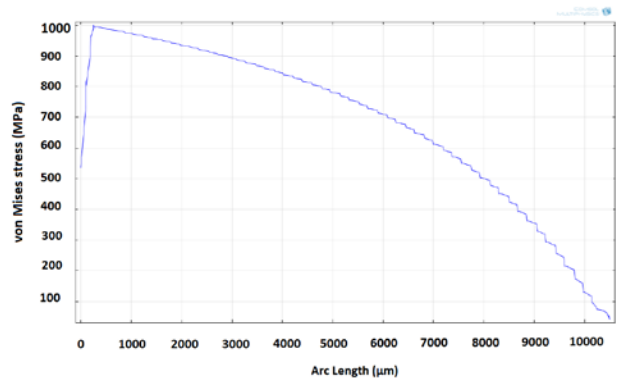

Figure 11. *Von Mises* stress induced upon applying a vertical force along the negative *z*-axis versus the electrode length (non-porous).

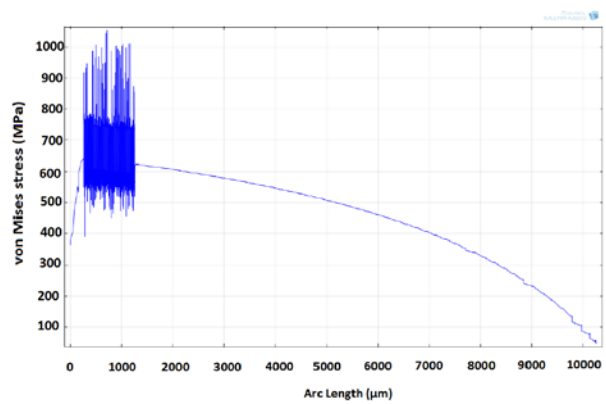

Figure 12: *Von Mises* stress induced upon applying a vertical force along the negative *z*-axis versus the electrode length (porous).

TABLE I. A COMPARISON OF FORCES THAT INDUCED 1GPA STRESS IN POROUS AND NON-POROUS ELECTRODES ALONG ALL THREE PRINCIPLE AXES.

Type of Force	Axis	Non-porous (mN)	Porous (mN)
Axial	Along –ve x	527.5	522.5
	Along –ve y	47.5	37.5
Vertical	Along ive z	18.25	11.5

Based on the mentioned results, since the forces needed to induce a maximum critical stress of 1GPa are less in the porous electrode than in the non-porous electrode, we can infer that the porous electrode is mechanically weaker than the non-porous electrode. This weakening is illustrated in Table 2.

TABLE II. RELATIVE WEAKENING OF POROUS ELECTRODE.

Weakening	**Axial (-ve x)**	**Axial (-ve y)**	**Vertical (-ve z)**
Percentage	0.1%	21%	37%

Additionally, it has been shown that the penetration force that an electrode must withstand is equal to 2.42±0.77 [12]. Since the forces that brought the porous electrode near failure are much higher than the force that the electrode must withstand during penetrating the brain tissue, we can deduce that the porous electrode would definitely survive the axial penetration force.

VI. CONCLUSION

We have presented the novel idea of the mechanical simulation of a porous neural electrode. Even though the introduction of the pores relatively weakened the neural electrode, the electrode was found still capable of surviving the brain environment. Nevertheless, certain limitations were present especially related to the finite element model. The full arrays of pores could not be simulated due to computational complexity and they were restricted to the weakest areas. Moreover, different radii of pores and volume porosity percentages should be tested. The porous electrode is superior to the non-porous electrode due to the improved biocompatibility and bioactivity it offers. Furthermore, the presence of the pores gives an additional advantage where they can behave as scaffolds for entrapping neural growth factors that encourage the re-growth of neurons. This alteration to the electrode's design is able to advance the healthcare services provided to neural diseases' patients all around the world.

REFERENCES

[1] K. C. Cheung, "Implantable microscale neural interfaces," Biomed Microdevices, vol. 9, 2007, pp. 923–938.
[2] R. Jung, Biohybrid systems: nerves, interfaces and machines: Wiley, 2012.
[3] B. He, Neural Engineering: Springer London, Limited, 2013.
[4] M. A. L. Nicolelis, "Brain–machine interfaces to restore motor function and probe neural circuits," Nature Reviews Neuroscience, vol. 4, 2003, pp. 417-422.
[5] P. F. G. B. Kim, and M. R. Abidian, "Electrode–neural tissue interactions: immune responses, current technologies, and future directions," in Biomaterials Surface Science, J. F. M. A. Taubert, and J. C. Rodriguez-Cabello, Ed., ed: Wiley-VCH, 2013.
[6] V. C. M. Hajj-Hassan, and S. Musallam, "NeuroMEMS: neural probe microtechnologies," Sensors, vol. 6704-6726, 2008, pp. 6704-6726.
[7] L. M. B. A. Rosengren, N. Danielsen, H. Persson , and M. Kober, "Tissue reactions to polyethylene implants with different surface topography," Journal of Materials Science: Materials in Medicine, vol. 10, 1999, pp. 75-82.
[8] L. W. A. Rosengren, N. Danielsen, T. Laurell, and L. M. Bjursten, "Tissue reactions evoked by porous and plane surfaces made out of silicon and titanium," IEEE Transactions on Biomedical Engineering, vol. 49, 2002, pp. 392-399.
[9] S. H. K. A. Moxon, A. Aslani , N. M. Kalkhoran, and P. I. Lelkes, "Bioactive properties of nanostructured porous silicon for enhancing electrode to neuron interfaces," Journal of Biomaterials Science, Polymer Edition, vol. 18, 2007, pp. 1263–1281.
[10] M. K.-K. M. Hajj-Hassan, H. Wang , V. Chodavarapu, and J. E. Henderson "Response of murine bone marrow-derived mesenchymal stromal cells to dry-etched porous silicon scaffolds," Journal of Biomedical Materials Research Part A, 2011, pp. 269-274.
[11] S. C. L. K. A. Moxon, G. A. Gerhardt, K. A. Barbee, and J. K. Chapin "Ceramic-based multisite electrode arrays for chronic single-neuron recording," IEEE Trans Biomed Eng., vol. 51, 2004, pp. 647-656.
[12] V. C. M. Hajj-Hassan, and S. Musallam, "Reinforced silicon neural microelectrode array fabricated using a commercial MEMS process," Journal of Micro/Nanolithography, MEMS, and MOEMS, vol. 8, 2009, pp. 033011-033018.
[13] A. Blake, Handbook of Mechanics, Materials, and Structures: Wiley, 1985.
[14] J. A. Collins, H. R. Busby, and G. H. Staab, Mechanical Design of Machine Elements and Machines: Wiley, 2010.